The Transfer Function of a Boreholed Dipole Antenna

Alina M. Badescu, *Member, IEEE*

***Abstract*— In this paper, a semiempirical model is presented to characterize the transfer function and scattering parameters of a vertical dipole antenna in the 164–174 MHz bandwidth. The antenna is either radiating in free space or it is inserted in an air-filled borehole in a salt mine. The model uses the signal flow graph for modeling of the antenna coupling with the environment and the effects of radio wave propagation in the layered medium. Analytical results are fit to measurements performed with a vector network analyzer, and the transfer functions are obtained by applying a least mean square algorithm. Experimental data acquired in free space allow also the determination of the intrinsic parameters of the antennas, providing a stand-alone method.**

***Index Terms*— Boreholed antenna, layered medium, transfer function.**

I. Introduction

THE behavior of antennas in different borehole environments is not well understood. Antenna's characterization is necessary for inverse problems to correctly identify the properties of natural dielectrics. Such analysis is performed before the construction of radio cosmic neutrino detectors in ice [1], salt [2], to detect buried objects, and to characterize the subsurface structure and properties in a wide variety of applications (e.g., archaeology, civil engineering, forensics, and geology [3]).

In borehole systems, the antenna acts as a filter so a transfer function must be associated with it [4]. The problem is not trivial because the propagation of radio waves in heterogeneous media is a subject not fully resolved [5] and the effect of antenna coupling with the medium cannot be isolated from the propagation model.

The problem of antennas radiating in the proximity of a dielectric medium was studied by several authors. Gentili and Spagnolini [6] addressed the problem of an antenna radiating above a layered medium, but the multiple reflections between the antenna and the medium were not accounted for. Other papers presented results for antennas in the 30–60 kHz range situated above the ground, at far-field distances [7]. Lambot and Andre [8] improved the model for a near-field scenario. Unfortunately, the algorithm is tested for a medium formed by two homogeneous layers (air and water) of a few centimeters each, thus the simulation complexity and time are small.

For antennas boreholed in dielectrics, the analysis is usually done using numerical methods to solve an integral equation for the current distribution. King and Smith [9] considered an approximate solution of this equation. The validation of King's expression through experimental measurements was done in [10]. Other attempts to model antennas in dielectrics were performed in [11]. Chen's more general model [12] gives unphysical input impedances of the antenna (negative input resistance) when the ambient medium is of low conductivity.

In the work addressed here, a semiempirical model is used to characterize the transfer function and the scattering parameters of a vertical dipole boreholed in a dielectric medium in the 164–174 MHz bandwidth. This bandwidth was chosen as a compromise between the radio wave penetration depth in the medium and the physical dimension of the antennas: lower frequencies allow larger propagation distances but require large antennas. Nonetheless, the dimensions of the antennas are limited by the size of the borehole, which in turn are constrained by the available drilling instrument. Even though measurements are performed in a bandwidth specific to a peculiar commercial antenna available on the market, the method can be applied to characterize any vertical dipole antenna boreholed in any dielectric medium.

The semiempirical model presented avoids a full analytical characterization of the antenna together with the numerical evaluation of Sommerfeld type integrals that account for propagation in layered media. Instead, the signal flow graph is used to describe the antenna coupling with the environment, together with the effects of radio wave propagation, while the antenna is described by a two-port network. The analytical model fits data measured with a vector network analyzer (VNA) to determine the unknown parameters, among which the transfer function of the antenna.

II. Model Formulation

The modeling of an antenna as a two-port network is not new. A valid two-port representation of an antenna must include the antenna's input impedance as well as its realized transfer function. Any antenna can be regarded as a two port [13] as indicated in Fig. 1. The radiation resistance R_{rad} is described by a transformer. Port 2 is terminated with the intrinsic impedance of the medium where the antenna radiates

Manuscript received February 27, 2018; revised June 21, 2018; accepted July 23, 2018. Date of publication August 8, 2018; date of current version October 29, 2018. This work was supported by European Research Council through the European Union's Horizon 2020 Research and Innovation Program under Grant 714637.

The author is with the Telecommunications Department, University Politehnica of Bucharest, 060042 Bucharest, Romania (e-mail: alinabadescu@radio.pub.ro).

Color versions of one or more of the figures in this paper are available online at http://ieeexplore.ieee.org.

Digital Object Identifier 10.1109/TAP.2018.2864340

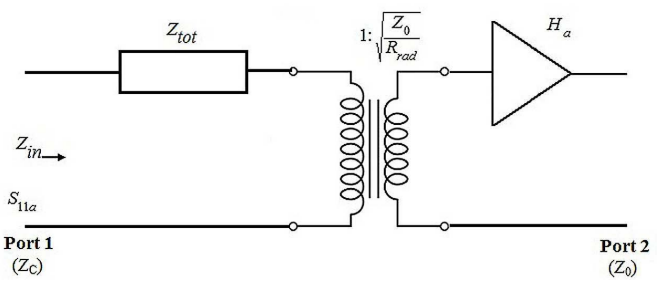

Fig. 1. Antenna as a two-port network.

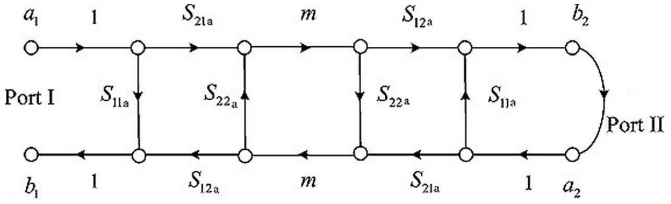

Fig. 2. Signal flow graph for a transmitting–receiving antenna system.

(e.g., $Z_0 = 120\pi\,\Omega$ for free space) and the characteristic impedance at port 1 is Z_c (50 Ω). The impedance Z_{tot} describes in a unitary form the intrinsic ohmic, dielectric and conduction losses of the antenna (Z_{int}), together with near-field associated losses. The antenna transfer function $H_a(f)$ included as an amplifier (or attenuator) stage.

The antenna transfer function concept is used in the literature in situations where the overall emitting–receiving system transfer function is necessary, especially when the propagation channel requires modeling [14], [15]. For simplicity, the antennas used should be identical and perfectly aligned such as to have identical transfer functions. Following the approach of [16], the transfer function is an intrinsic attribute of the antenna, defined independently on the distance between the transmitter and receiver (and this is can be observed in Fig. 1). The transfer function describes antenna behavior in frequency and it might incorporate other factors also (i.e., polarization and gain).

Referring to Fig. 1, the S_{11a} parameter represents the reflection coefficient at the antenna input (the index a will be used to refer to a parameter of the antenna from now on). All the parameters of the scattering matrix can be determined analytically from the two-port model once the transfer function H_a is known.

Regardless the type of antenna, the intrinsic impedance Z_{int} can only be measured experimentally. For that I have used an emission (Tx)–reception (Rx) system, and the measurements have been performed in free space (a detailed description of the measurements is presented in Section III-A). The antennas were identical, such as the scattering parameters are the same, and perfectly aligned to exclude polarization losses.

A particularly useful technique that can be used to study the physical networks is the signal flow graph. The technique provides a solution to the network equations using a systematic procedure [17]. The signal flow diagram of the Tx–Rx antenna system together with the effect of the propagation medium in between is presented in Fig. 2. Port 1 represents the transmitting port and port 2 represents the receiving one (this convention will be used from now on throughout this paper). The free-space factor is [14]

$$m = \frac{\exp(-jk_0r_0)}{4\pi r_0} \tag{1}$$

where r_0 is the distance between the emitting and receiving antenna and the wavenumber k_0 is equal to $k_0 = 2\pi/\lambda_0$, λ_0 being the wavelength in free space.

The scattering parameters of the overall system can be determined from the graph flow, using Masons' rules [17]. The graph has only one closed loop, whose transmittance is $m^2 \cdot S_{22a}^2$. Following the direction of the arrows (that indicate the propagation direction), the reflection coefficient at port 1 and the transmission coefficient from port 1 to port 2 can be calculated analytically

$$S_{11,sys} = S_{11,a} + \frac{S_{21a} \cdot S_{12a} \cdot m^2}{1 - m^2 \cdot S_{22a}^2} \tag{2}$$

$$S_{21,sys} = \frac{S_{21a} \cdot S_{12a} \cdot m}{1 - m^2 \cdot S_{22a}^2} \tag{3}$$

and can be measured directly with a VNA.

If the medium where the antennas radiate is more complex (such as a salt dome), the signal flow graph should be modified to characterize all the phenomena that occur at propagation, and this is the subject in Section II-A.

A. Heterogeneous Propagation Environment

The salt deposit, where the measurements for this paper were carried out, is the result of layers of dried solutes from ancient seas that suffered deformation through tectonic and buoyant forces (i.e., a salt diaper). Each layer has different thickness and dielectric characteristics according to the nature of the deposited sediments, which are not normally known. This is one of the main reasons why the problem addressed in this paper is difficult to solve, as commercial analysis software for antenna and propagation description require as input of exactly the mentioned unknown quantities. Some recent work using detailed finite difference time domain models [18] presented simulations for lossy heterogeneous environments, but there the medium was continuous, which already excludes the main source of power losses, reflections at interfaces of separation [19].

When layering is present, the reflections at the different interfaces may interfere in a constructive or destructive way [20]. For the salt rock, in the 164–174 MHz bandwidth, any layer of $\approx$ 20 cm will cause a maximum/minimum interference. Moreover, any layer with a thickness smaller than 40 cm can produce reflections (to obtain these figures, the permittivity of the layer was approximated to $\epsilon_r = 6$, a common figure used for salt [21]).

Other propagation effects, such as scatterings on impurities, have been estimated elsewhere [19] and their overall effect on

the attenuation of radio waves is very small compared to other effects (e.g., reflections at interfaces of separation between layers).

In this paper, it was considered that the propagation medium is formed by nearly parallel nondispersive layers of sediments in the 164–174 MHz bandwidth (this layer distribution was observed at the site of the experiment).

The radio waves were transmitted and received by vertical dipole antennas placed in boreholes in salt filled with air, parallel to the layers of sedimentary salt, and separated by a distance d of 10 m. The waves emitted by the Tx antenna propagate first in the air in the borehole, thus a first reflection will occur at the interface between air and the first layer of salt. The reflection coefficient at this first interface is R_1 and depends on the complex permittivity of the first layer of salt ϵ_1. Afterward each layer of salt will produce a new reflection, $R_i, i > 2$. The model also includes multiple reflections within each layer. The attenuation between interfaces $i-1$ and i is $F_{(i-1)i}$, and it depends on: the thickness of the layer and the permittivity of the layer. The dependence on the incidence angle has not been explicitly written because it is beyond the purpose of this paper: here all reflections and attenuations (or expressions that contain combinations of them) are extracted from measurements.

To conclude, when a layered medium of propagation is considered (2) and (3) should be modified as

$$S_{11,sys} = S_{11,as} - \frac{S_p}{S_{22,as}} + T \tag{4}$$

$$S_{21,sys} = \frac{S_p \cdot F_{12} \cdot F_{23} \cdots F_{nn+1} A_{n+1}}{\Delta} \tag{5}$$

where

$$S_p = S_{12,as} \cdot S_{21,as}$$

and

$$T = 2\ S_p R_1 \left(1 + \frac{S_{22,as} \cdot R_1 - 1}{\Delta}\right) + \frac{S_p}{S_{22,as} \cdot \Delta}.$$

In (5), $n+1$ is the last interface (salt– air) and A_{n+1} represents the transmission coefficient in the air of the borehole of the receiving antenna (assumed to be equal to 1 since the diameter of the hole is only 7.5 cm). The quantity Δ is

$$\Delta = 1 - S_{22,as}\left[R_1 + R_2 \cdot F_{12}^2 + R_3 \cdot F_{12}^2 \cdot F_{23}^2 + \cdots\right]. \tag{6}$$

In (4)–(6), the index s has been introduced to refer to the scattering parameters of an antenna when placed in a borehole in salt. Also, note that $S_{ij,a} \neq S_{ij,as}$ (the equality of the two terms was suggested in [22]).

The derivation of last equations is based on Masons' rules [17]. Each reflection at separation borders creates a new transmission loop, easily observed in (6); there are no second-order or higher order loops in the system. However, each of the newly created loops touches a forward path, either from port 1 to port 1 or from port 1 to port 2, preventing it to appear in the expression for $S_{11,sys}$ or $S_{21,sys}$. The only exception for a reflection coefficient is $S_{22,as}R_1$, and this is the reason why R_1 is displayed in (4). The transmission from port 1 to port 2 consists of only one possible path as shown in (5).

The scattering parameters of the antenna when it radiates in salt can be deduced from the two-port scheme of the antenna, adapted after Fig. 1. The scattering parameters depend on the medium where the antenna radiates (medium defined by its far-field dielectric characteristics) but not on the distance between emitter and receiver. The characteristic impedance at port 2 is the dielectric impedance of the surrounding medium (with an overall equivalent complex permittivity ϵ_r that describes the far-field conditions). The impedance $Z_{tot,s}$ includes the intrinsic properties of the antenna (Z_{int}, that depends only on the antenna and not on the medium when the antenna radiates), and the loading caused by the natural dielectric. The loading itself can be quantified in a complex impedance at the antenna feed point [23]. The radiation resistance in salt is marked by $R_{rad,s}$, and the antenna transfer function by $H_{a,s}$. With the exception of Z_{int}, all parameters are different when antennas radiate in the air, compared to salt, and should be determined experimentally.

The input impedance of an antenna in an air-filled borehole in a dielectric medium was determined in [24]

$$Z_{in} = \frac{Z_0 \Psi(k)}{2\pi\sqrt{\epsilon_r}}\left[1 + \frac{1}{jkh} - 2\frac{\Phi'(x)}{\Phi(x)}\right] \tag{7}$$

where $\Phi(x) = F_1(1-\alpha, 2, x)$ is related to the confluent hypergeometric function and Φ' is its derivative with respect to x, α is the square root of the permittivity of the medium ϵ_r, $k = k_0\sqrt{\epsilon_r}$, $x = -2jkh$, where h is equal to the half of the length of the antenna. The function Ψ was determined in [25]

$$\Psi(k) = 2\left[\sinh^{-1}\left(\frac{h}{a}\right) - C_i(2ka, 2kh) - jS_i(2ka, 2kh)\right] + A \tag{8}$$

with

$$A = j\frac{1 - \exp(-2jkh)}{kh}.$$

C_i (S_i) are the generalized cosine (sine) integral functions and a is antenna's radius.

III. Measurements and Results

All measurements were performed using a VNA, produced by Deviser, model NA7300A, that recorded the S-scattering parameters between the input and output ports (both with a characteristic impedance of 50 Ω).

The pair of omnidirectional dipoles used for measurements was produced by Kathrein, model K552628 (164−174 MHz). Antenna's total length was 993 mm, the radius equal to 3.509 cm, it had a vertical polarization and gain of 2 dBi. According to the manufacturer, the antenna exhibits an omni-directional pattern in the horizontal plane, while in the vertical plane it has a 3 dB angle of 78°, centered on the direction normal to the antenna. The input impedance of the antenna is 50 Ω.

For connections to the ports of the VNA, 50 Ω N-type coaxial cables (EC400 +) were used. Other two coaxial cables (RG 58) of 1 m length each were used to interconnect the SMA input–output of an amplifier with the Rx antenna. The effects of the RG 58 cables were excluded in the data postprocessing.

The amplifier used was produced by Aaronia, model UBBV1, with a gain of about 40 dB in the 50 MHz–1 GHz band. The exact values of the gain of the amplifier at each frequency were extracted from the data sheet provided by the manufacturer.

The frequency-dependent complex ratios $S_{11}(f)$ and $S_{21}(f)$ between the returned signal/transmitted signal and the emitted signal (corresponding to (2) and (3) for measurements in air, and (4) and (5) for measurements in salt) were measured sequentially at the maximum number allowed by the VNA, 1601 evenly stepped operating frequencies in the nominal frequency band. The sweep time was set to 2 s to increase the accuracy of the measurements, and an averaging factor of 10 was chosen to improve the signal-to-noise ratio. The system had a constant transmission power of 10 dBm.

To reduce the systematic errors, the measurement setup was kept the same for measurements in free space, and also when the antennas were placed in boreholes in salt. The reflection losses caused by the connection of most cables (together with changes in the measurement reference planes) were removed by a null calibration of the VNA.

A. Measurements in Free Space

The main purpose of measurements in free space was to determine the intrinsic properties of the commercial antennas (e.g., Z_{int}). All the measurements were performed in the main chamber of the salt mine "Unirea" (Slanic Prahova, Romania).

The main chamber has a height of 50 m and a surface larger than 5000 m^2 [26]. It is a radio quiet zone because it is situated at 208 m depth and the soil above (more than 50 m thick) absorbs all man-made or natural radio frequencies. However, the reflections from the floor of the chamber and the measuring instrumentation could not be avoided. The noise level inside the chamber was measured with the VNA, and a mean value of -97 dB was found in the 164–174 MHz band.

In the measurement setup, the receiving and transmitting antennas were connected to the ports of the VNA.

The distance between antennas (i.e., the propagation distance) measured accurately with a laser tape was $r_0 = 11.7$ m.

The reflection and transmission coefficients between the two ports of the analyzer were measured and by using (2) and (3) together with the two-port model of the antenna, the intrinsic parameters of the antenna were determined. For the radiation resistance and the losses associated with near-field effects, the standard formulas for a sleeve dipole were used [27].

The variation with frequency of the complex intrinsic impedance Z_{int} was determined and it is represented in Fig. 3.

The modulus and phase of the antenna transfer function H_a were also determined and are presented in Fig. 4.

B. Measurements in Salt

The measurements with antennas positioned in boreholes were also performed in the main chamber on "Unirea" salt mine. The mine itself is positioned as such the thickness of the salt walls is larger than 100 m, and there are more than 100 m of salt below and above the holes.

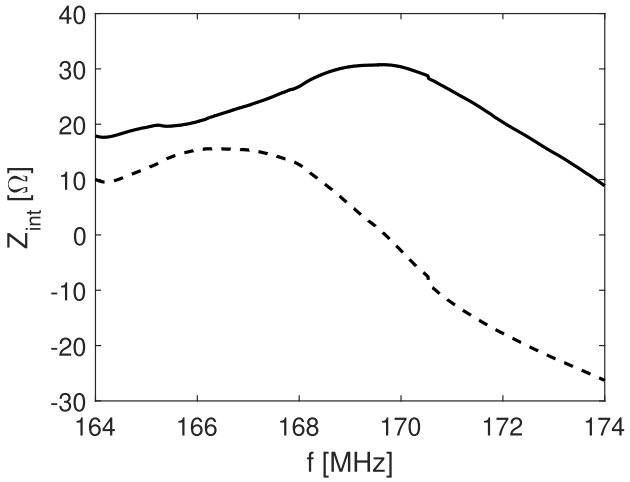

Fig. 3. Impedance of the antenna. Solid line: resistance loss. Interrupted line: reactance of the antenna.

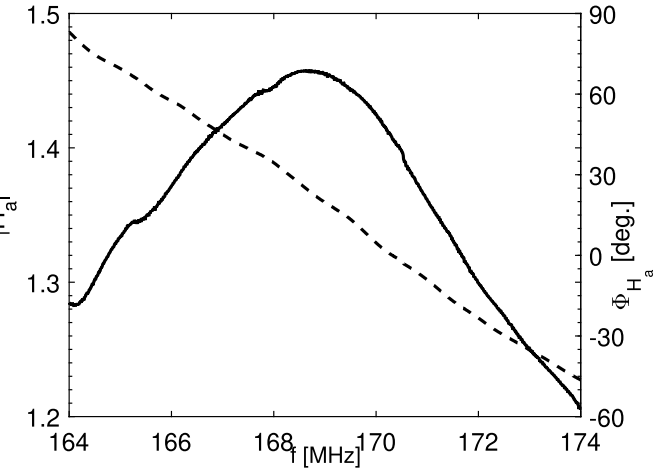

Fig. 4. Antenna transfer function in air. Left y–axis: modulus of the transfer function (continuous line). Right y–axis: phase of the transfer function (interrupted line).

To measure the attenuation of radio waves in natural salt, two cylindrical holes separated by 10 m were drilled in a wall. The holes have been drilled parallel to each other, at the same height from the chamber floor, each hole having a total depth of 1.2 m and a diameter of 75 mm. The emitter and receiver antennas were inserted into the borehole and connected to the ports of the VNA (Fig. 5). The Rx antenna was followed by an amplifier. Again $S_{11}(f)$ and $S_{21}(f)$ were measured in 1601 frequency points in the nominal band.

The distance of 10 m between the boreholes was chosen to meet the far-field measurement criteria. In an *a priori* calculus, the permittivity of the medium has been considered in the 5–7 range for determining the far-field limit. A safety margin was also added.

The analytical model represented by (4)–(8), combined with the scattering parameters of the antennas $S_{ij,as}$ determined from the two-port model of the antennas in salt should fit the measured data in order to determine the unknown quantities. Even though the goal of this paper is to determine the transfer

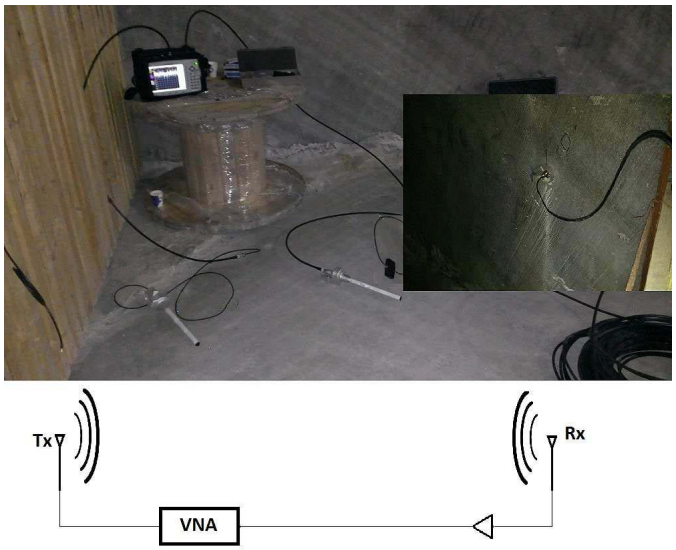

Fig. 5. Measurement principle. In the lower part of the picture, a schematic shows that the Tx an Rx antennas are connected to the two ports of the VNA (the antenna at reception is followed by an amplifier). The upper part of the picture presents the actual instrumentation used. Each antenna is inserted into a hole drilled in the wall of the mine chamber, as shown in a detail in the right-hand side of the figure. The distance between the Tx–Rx antennas is 10 m.

function $H_{a,s}$ (that is included in the $S_{ij,as}$ scattering parameters), the indefinite system of equations requires estimation of all variables simultaneously. All parameters involved are complex numbers, which doubles the number of unknowns.

This is the main reason why a classical Levenberg–Marquardt fitting algorithm is unusable. The approach in this paper is outlined in the next paragraphs.

The first part of the algorithm uses the two-port model of the antenna combined with (7) and the previously determined Z_{int} (shown in Fig. 3) to calculate a 3-D matrix with possible values for the radiation resistance in salt, $[R_{rad,s}(\epsilon_r, f)]$. In the second step, a fitting algorithm combines measurements S_{11} with (4) to determine the complex quantities: $[H_{a,s}]$, $[\Delta]$, and $[R_1]$ using the least mean square method. Results are also 3-D matrices, depending on frequency and complex permittivity ϵ_r. The last part of the numerical algorithm uses (5) to calculate the product $\prod_{i=2}^{n+1} F_{(i-1)i}$ based on measurements S_{21} and the 3-D matrices determined in the previous step. Finally, the condition $|\prod_{i=2}^{n+1} F_{(i-1)i}| < 1$ constraints the value of ϵ_r (the terms $F_{(i-1)i}$ represent attenuations).

The equivalent permittivity for the far-field conditions was determined to be $\epsilon_r = 5.667 - j0.0169$. A value of 5.663 was obtained in [28] for the real part of the permittivity from laboratory measurements of salt samples (a comparison of the imaginary parts is not relevant because in [28], the samples were doped with a small concentration of single type impurities, which is not the case here).

Based on the result obtained for the permittivity, the antenna transfer function was extracted from the 3-D matrix $[H_{a,s}]$. The function includes yet another effect that has not been mathematically modeled: the effect of scattering on impurities. Even though the overall effect in terms of amplitudes is small, each scattering will produce a phase shift [5].

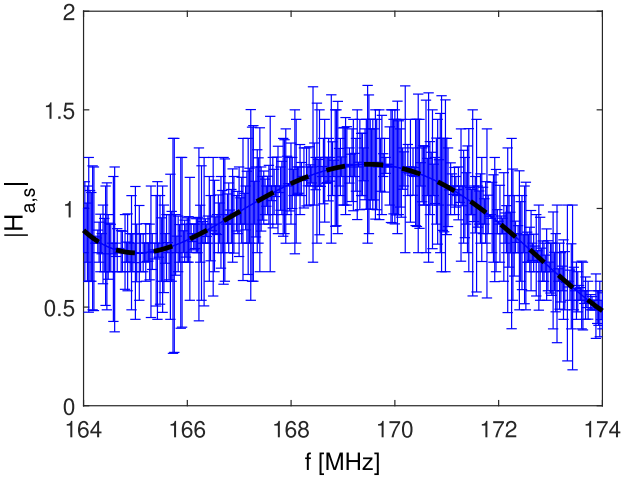

Fig. 6. Modulus of the transfer function when antenna is inserted in a borehole in salt.

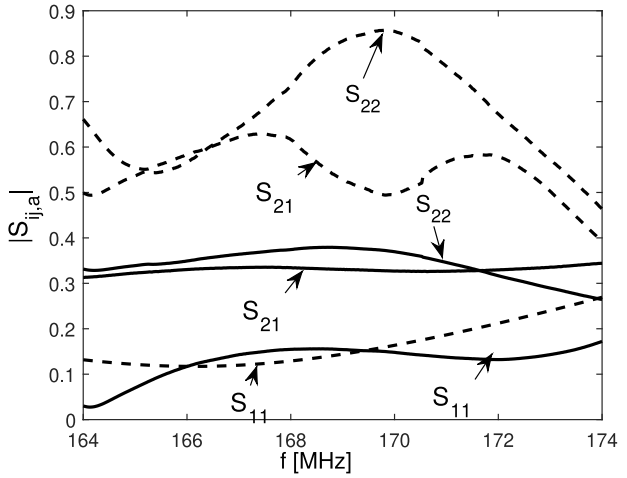

Fig. 7. Determined scattering parameters of the antenna when it radiates in air (continuous line) and salt (dashed line).

A χ^2 test was performed; constraint by the fact that the transfer function should remain a continuous function. The modulus of the transfer function was determined and it is represented in Fig. 6. The dashed curve represents the best fit. The types of impurities and their concentration within each layer vary and are unknown, thus the effect on the phases cannot be estimated nor reconstructed.

Once the transfer function $|H_{a,s}|$ was determined with the help of measurements, the scattering parameters of the antenna $S_{ij,as}$ can be determined from the two-port model of the antenna. For illustrative purposes, Fig. 7 shows in a unitary form the reconstructed scattering parameters of the antenna in a fixed bandwidth, when the antenna radiates in the air (continuous line) and when the antenna is in a borehole in salt (dashed line).

Another aspect that should be discussed is the resonance frequency of the antenna. The resonance frequency, as a standard definition, is the frequency for which the reactance of the antenna equals zero or is near zero.

When an antenna radiates in a dielectric medium, the presence of the medium affects the current distribution on

the antenna. The current velocity along the antenna varies, thus changing (lowering) the resonance frequency [3]. More to this, the electrical impedance of an antenna is lower in a dielectric medium and this reflects in a drop in the central frequency of the antenna [29].

If the antenna radiates in the proximity of a dielectric medium, the wave velocity will have a value between the velocity of an electromagnetic wave in the air and in the medium [30]. In [31], it is proven in a very elegant way that in a half-spaces problem the drop in frequency will scale with $n^3/(1+n)^2$ (in the direction of interest for this paper), n being the refraction index of the dielectric medium.

Simulations regarding the resonance frequency of an antenna submerged in an ideal, homogeneous dielectric (characterized by $\Re\{\epsilon_r\} = 5.8$ and a conductivity $\sigma = 0.001$ S/m) shown that the antenna exhibits actually two resonance frequencies [23]. The same work reported that when the antenna is introduced in an air-filled borehole (i.e., it does not radiate directly in the medium) the resonance frequencies are shifted toward larger values, with values between 24 to 33 MHz (these values where obtained from simulations in which the dimension of the borehole was 10 cm).

Measurements reported in this paper show that the antenna is resonant on 169.7 MHz when it radiates in the air, and exhibits one resonance at 167.6 MHz when is radiating in an air-filled borehole in salt (the other resonance is outside the measured bandwidth). This is consistent with results from [31] which show that the central frequency in a half-spaces scenario should be around 143 MHz, which should be shifted upward with more than 20 MHz due to the presence of the borehole.

IV. Conclusion and Discussion

In this paper, the magnitudes of the transfer function and the characteristic scattering parameters of a vertical dipole boreholed in natural rock salt were determined with the help of a semiempirical model. The scattering parameters allow a full characterization of the functionality of commercial antennas in a certain frequency bandwidth, which can be directly used in inverse problems. The dipole antenna was chosen because it radiates a symmetric radiation pattern relative to the horizontal plane at their feed point that helps in the detection of a multilayered structure.

The typical method for dealing with layered media requires a numerical evaluation of Sommerfeld type integrals. If the layers have a thickness of a few centimeters, and the overall propagation length is at the order of tens of meters, the method is inapplicable from the simulation time perspective. A large number of unknowns could even make the method nonconvergent. The model addressed here eliminates this inconvenient. Moreover, the empirical results estimate all the near-field phenomena (associated with losses) that no longer have to be analytically modeled or simulated with specific software.

The internal impedance of the antenna was determined by measurements in free space. Although properties of antennas are usually measured in anechoic chambers, for the 164–174 MHz bandwidth there are just a few such facilities and not available for the public in Romania. This is the reason why measurements were performed in the low noise main chamber of the mine, in an area where no reflecting objects were present. However, the reflections from the floor of the chamber and the measuring instrumentation could not be avoided.

Another aspect that required investigation was that due to the limitations from the drilling tool (that dictated the dimensions of the borehole, including its height), the dipoles were situated very close to a reflecting plane perpendicular to the antennas (the interface between the salt wall and air). This had mainly two effects: a complex loading at the input of the antenna (that was considered in the model) and secondary lobes that result in power loss.

A complete analysis of complex image theory in nonperfect media is presented in [32]. Due to the small diameter of the boreholes relative to the wavelength, propagation of energy along the borehole is small and limited to very high frequencies [33].

The small losses were confirmed by simulations in [23] which show that a dipole antenna in an air-filled borehole in salt, with one end close to the ground plane, would produce one secondary lobe with an amplitude less than a quarter of that of the main lobe. The direction of the maximum of the main lobe remained the same but the half-power beamwidth angle decreased to about 60° (compared to 78° in free space).

Some measurements of the losses have been done also at the site of the experiment (i.e., losses in terms of the waves emitted by an antenna in the borehole in salt that propagates in air). It was calculated that the mean power emitted through free space was $\approx 50\times$ smaller than the mean power transmitted through salt, thus the proximity of the reflecting plane (the interface between the salt wall and air) does not significantly influence the results reported in this paper.

The effect of an off-centered antenna has been estimated by repeating the measurements in several campaigns. The antennas were introduced in the boreholes, parallel and centered. The magnitude of the recorded S_{21} varied by less than 0.5 dB, while the phase with less than 2°, in all bandwidth. It was concluded that small, unintentional unalignment does not influence the final results.

The only effect that cannot be completely modeled and removed in data postprocessing is the scattering of impurities. Not only the concentration of impurities within each layer is unknown but also the type of impurities within each layer is unknown. This results in the impossibility to reconstruct the phases of the transfer function and scattering parameters, as the uncertainty is too high to allow a significant fitting.

Acknowledgment

The author would like to thank the Romanian National Salt Company for the help provided with the operations in "Unirea" salt mine in Slanic Prahova, Romania. She would also like to thank the reviewers for their valuable comments.

References

[1] P. Allison *et al.*, "Design and initial performance of the Askaryan Radio Array prototype EeV neutrino detector at the South Pole," *Astroparticle Phys.*, vol. 35, no. 7, pp. 457–477, Feb. 2012.

[2] A. Connolly, A. Goodhue, C. Miki, R. Nichol, and D. Saltzberg, "Measurements of radio propagation in rock salt for the detection of high-energy neutrinos," *Nucl. Instrum. Methods Phys. Res. A, Accel. Spectrom. Detect. Assoc. Equip.*, vol. 599, nos. 2–3, pp. 184–191, Feb. 2009.
[3] D. J. Daniels, Ed., *Ground Penetrating Radar*, 2nd ed. London, U.K.: Institution of Engineering and Technology, 2004.
[4] S. Zwierzchowski and P. Jazayeri, "A systems and network analysis approach to antenna design for UWB communications," in *Proc. IEEE Antennas Propag. Soc. Int. Symp.*, vol. 1, Jun. 2003, pp. 826–829.
[5] B. Hapke, *Theory of Reflectance and Emittance Spectroscopy*. Cambridge, U.K.: Cambridge Univ. Press, 1993.
[6] G. G. Gentili and U. Spagnolini, "Electromagnetic inversion in monostatic ground penetrating radar: TEM horn calibration and application," *IEEE Trans. Geosci. Remote Sens.*, vol. 38, no. 4, pp. 1936–1946, Jul. 2000.
[7] D. Moghadas, F. André, H. Vereecken, and S. Lambot, "Efficient loop antenna modeling for zero-offset, off-ground electromagnetic induction in multilayered media," *Geophysics*, vol. 75, no. 4, pp. 125–134, 2010.
[8] S. Lambot and F. André, "Full-wave modeling of near-field radar data for planar layered media reconstruction," *IEEE Trans. Geosci. Remote Sens.*, vol. 52, no. 5, pp. 2295–2303, May 2014.
[9] R. W. P. King and G. S. Smith, *Antennas in Matter: Fundamentals, Theory, and Applications*. Cambridge, U.K.: MIT Press, 1981.
[10] M. Sato and R. Thierbach, "Analysis of a borehole radar in cross-hole mode," *IEEE Trans. Geosci. Remote Sens.*, vol. 29, no. 6, pp. 899–904, Nov. 1991.
[11] S. Ebihara and W. C. Chew, "Calculation of Sommerfeld integrals for modeling vertical dipole array antenna for borehole radar," *IEICE Trans. Electron.*, vol. E86-C, no. 10, pp. 2085–2096, 2003.
[12] K. C. Chen and L. K. Warne, "A uniformly valid loaded antenna theory," *IEEE Trans. Antennas Propag.*, vol. 40, no. 11, pp. 1313–1323, Nov. 1992.
[13] S. D. Rogers, J. T. Aberle, and D. T. Auckland, "Two-port model of an antenna for use in characterizing wireless communications systems, obtained using efficiency measurements," *IEEE Antennas Propag. Mag.*, vol. 45, no. 3, pp. 115–118, Jun. 2003.
[14] A. O. Boryssenko and D. H. Schaubert, "Antenna link transfer function factorization applied to optimized channel design," *IEEE Trans. Antennas Propag.*, vol. 54, no. 10, pp. 2878–2889, Oct. 2006.
[15] A. H. Mohammadian, A. Rajkotia, and S. S. Soliman, "Characterization of UWB transmit-receive antenna system," in *Proc. IEEE Conf. Ultra Wideband Syst. Technol.*, Reston, VA, USA, Nov. 2003, pp. 157–161.
[16] S. Zwierzchowski and P. Jazayeri, "Derivation and determination of the antenna transfer function for use in UWB communication analysis," in *Proc. 15th Int. Conf. Wireless*, Calgary, AB, Canada, 2003, pp. 533–543.
[17] S. R. Pennock and P. R. Shepherd, *Microwave Engineering With Wireless Applications*. London, U.K.: McGraw-Hill, 1998.
[18] C. Warren and A. Giannopoulos, "Characterisation of a ground penetrating radar antenna in lossless homogeneous and lossy heterogeneous environments," *Signal Process.*, vol. 132, pp. 221–226, Mar. 2017.
[19] A.-M. Badescu, "Considerations on an underground neutrino radio detector in salt," *J. Instrum.*, vol. 8, p. P03010, Mar. 2013.
[20] L. D. Landau, L. P. Pitaevskii, and E. M. Lifshitz, *Electrodynamics of Continuous Media*, vol. 8, 2nd ed. Amsterdam, The Netherlands: Elsevier, 1984.
[21] M. C. Robinson and A. C. Hollis Hallett, "The static dielectric constant of NaCl, KCl, and KBr at temperatures between 4.2 °K and 300 °K," *Can. J. Phys.*, vol. 44, no. 10, pp. 2211–2230, 1966.
[22] E. Slob, M. Sato, and G. Olhoeft, "Surface and borehole ground-penetrating-radar developments," *Geophysics*, vol. 75, no. 5, pp. 103–120, 2010.
[23] S. Liu and M. Sato, "Transient radiation from an unloaded, finite dipole antenna in a borehole: Experimental and numerical results," *Geophysics*, vol. 70, no. 6, pp. K43–K51, 2005.
[24] L.-C. Shen and T. T. Wu, "Cylindrical antenna with tapered resistive loading," *Radio Sci.*, vol. 2, no. 2, pp. 191–201, Feb. 1967.
[25] T. Wu and R. King, "The cylindrical antenna with nonreflecting resistive loading," *IEEE Trans. Antennas Propag.*, vol. AP-13, no. 6, pp. 369–373, May 1965.
[26] *National Romanian Salt Company*. Accessed: Feb. 20, 2018. [Online]. Available: http://www.salrom.ro/slanic-prahova-baza-turistica.php
[27] J. Kraus and R. Marhefka, *Antennas for all Applications*, 3rd ed. New York, NY, USA: McGraw-Hill, 2003.
[28] B. Meng, B. D. B. Klein, J. H. Booske, and R. F. Cooper, "Microwave absorption in insulating dielectric ionic crystals including the role of point defects," *Phys. Rev. B, Condens. Matter*, vol. 53, p. 12777, May 1996.
[29] S. G. Millard, A. Shaari, and J. H. Bungey, "Field pattern characteristics of GPR antennas," *NDT&E Int.*, vol. 35, no. 7, pp. 473–482, 2002.
[30] F. I. Rial, H. Lorenzo, M. Pereira, and J. Armesto, "Waveform analysis of UWB GPR antennas," *Sensors*, vol. 9, no. 3, pp. 1454–1470, 2009.
[31] N. Engheta, C. H. Papas, and C. Elachi, "Radiation patterns of interfacial dipole antennas," *Radio Sci.*, vol. 17, no. 6, pp. 1557–1566, 1982.
[32] C. R. Liu, *Theory of Electromagnetic Well Logging*. Amsterdam, The Netherlands: Elsevier, 2017.
[33] J. W. Lane, P. K. Joesten, G. Pohll, and T. Mihevic. (2001). *Analysis of Borehole-Radar Reflections Logs From Selected HC Boreholes at the Project Shoal Area, Churchill Country, Nevada*. Accessed: Feb. 20, 2018. [Online]. Available: https://water.usgs.gov/ogw/bgas/publications/wri014014/wri014014.pdf

Alina M. Badescu (M'09) received the B.Sc. degree in electrical engineering from the University Politehnica of Bucharest, Bucharest, Romania, in 2006, the M.Sc. degree in radio astronomy and space science from Chalmers University, Gothenburg, Sweden, in 2008, and the Ph.D. degree from the University Politehnica of Bucharest, in 2011.

She is currently an Associate Professor with the Department of Telecommunications, University Politehnica of Bucharest. She has been involved in several research projects, mainly regarding radio frequency systems. She has authored and co-authored over 50 peer-reviewed journals, conference papers, and two books.

Dr. Badescu has been the Vice Chair of the IEEE Antenna and Propagation Chapter-Romania, since 2017.